The Journal of Immunology

Intratumoral hu14.18–IL-2 (IC) Induces Local and Systemic Antitumor Effects That Involve Both Activated T and NK Cells As Well As Enhanced IC Retention

Richard K. Yang, Nicholas A. Kalogriopoulos, Alexander L. Rakhmilevich, Erik A. Ranheim, Songwon Seo, KyungMann Kim, Kory L. Alderson, Jacek Gan, Ralph A. Reisfeld, Stephen D. Gillies, Jacquelyn A. Hank and Paul M. Sondel

J Immunol 2012; 189:2656-2664; Prepublished online 27 July 2012;
doi: 10.4049/jimmunol.1200934
http://www.jimmunol.org/content/189/5/2656

The Journal of Immunology is published twice each month by
The American Association of Immunologists, Inc.,
1451 Rockville Pike, Suite 650, Rockville, MD 20852

Print ISSN: 0022-1767 Online ISSN: 1550-6606.

Intratumoral hu14.18–IL-2 (IC) Induces Local and Systemic Antitumor Effects That Involve Both Activated T and NK Cells As Well As Enhanced IC Retention

Richard K. Yang,[*,1] Nicholas A. Kalogriopoulos,[*,1] Alexander L. Rakhmilevich,[*,†] Erik A. Ranheim,[†,‡] Songwon Seo,[†,§] KyungMann Kim,[†,§] Kory L. Alderson,[*] Jacek Gan,[*] Ralph A. Reisfeld,[¶] Stephen D. Gillies,[‖] Jacquelyn A. Hank,[*,†] and Paul M. Sondel[*,†,#]

hu14.18–IL-2 (IC) is an immunocytokine consisting of human IL-2 linked to hu14.18 mAb, which recognizes the GD2 disialoganglioside. Phase 2 clinical trials of i.v. hu14.18–IL-2 (i.v.-IC) in neuroblastoma and melanoma are underway and have already demonstrated activity in neuroblastoma. We showed previously that intratumoral hu14.18–IL-2 (IT-IC) results in enhanced antitumor activity in mouse models compared with i.v.-IC. The studies presented in this article were designed to determine the mechanisms involved in this enhanced activity and to support the future clinical testing of intratumoral administration of immunocytokines. Improved survival and inhibition of growth of both local and distant tumors were observed in A/J mice bearing s.c. NXS2 neuroblastomas treated with IT-IC compared with those treated with i.v.-IC or control mice. The local and systemic antitumor effects of IT-IC were inhibited by depletion of NK cells or T cells. IT-IC resulted in increased NKG2D receptors on intratumoral NKG2A/C/E$^+$ NKp46$^+$ NK cells and NKG2A/C/E$^+$ CD8$^+$ T cells compared with control mice or mice treated with i.v.-IC. NKG2D levels were augmented more in tumor-infiltrating lymphocytes compared with splenocytes, supporting the localized nature of the intratumoral changes induced by IT-IC treatment. Prolonged retention of IC at the tumor site was seen with IT-IC compared with i.v.-IC. Overall, IT-IC resulted in increased numbers of activated T and NK cells within tumors, better IC retention in the tumor, enhanced inhibition of tumor growth, and improved survival compared with i.v.-IC. ***The Journal of Immunology*****, 2012, 189: 2656–2664.**

Immunocytokines are synthetic fusion proteins that consist of tumor-specific mAbs linked to an immune-stimulating cytokine. hu14.18–IL-2 (IC), originally created and described by Gillies et al. (1), is an immunocytokine consisting of human IL-2 linked to each IgG H chain of the hu14.18 mAb, which recognizes the GD2 disialoganglioside present on tumors of neuroectodermal origin (i.e., neuroblastoma, melanoma) (1). Immunocytokines are capable of augmenting significant antitumor effects in murine models by targeting the therapy to the tumor and stimulating the immune system to selectively destroy the cancer cells. In a syngeneic A/J murine model of neuroblastoma, the i.v. administration of the anti-GD2 ch14.18–IL-2 fusion protein induced a cell-mediated antitumor response that eradicated established bone marrow and liver metastases more efficiently than did equivalent mixtures of Ab and recombinant human IL-2 (2). The effector mechanism involved was shown to be exclusively dependent on NK cells (3). In a syngeneic BALB/c model, the huKS1/4–IL-2 immunocytokine, a humanized Ab against epithelial cell adhesion molecule (EpCAM) linked to IL-2, was used to elicit a T cell-mediated eradication of established pulmonary and hepatic CT26-KSA murine colon carcinoma metastases (4). Again, mixtures of mAb huKS1/4 with recombinant human IL-2 were less effective and only partially reduced tumor load (4). In a human melanoma (A375GFP) xenograft murine model, the immunocytokine scFvMEL/TNF, a fusion of human TNF and an Ab single-chain variant fragment (scFv) against the melanoma gp240 Ag (scFvMEL), targets melanoma cells in vivo and results in pronounced antitumor effects after systemic administration (5).

Clinical trials involving predecessors to the immunocytokine IC to treat GD2$^+$ tumors, such as neuroblastoma, have shown progress in recent years. A recent phase 3 trial using a chimeric anti-GD2 mAb (ch14.18) in combination with IL-2, GM-CSF, and 13-cisretinoic acid showed an increase (66 versus 46%) in event-free survival in pediatric neuroblastoma patients over the previous standard-of-care maintenance therapy, 13-cisretinoic acid (6). IC itself has also shown clinical activity in children with recurrent, refractory neuroblastoma. A phase I clinical trial sponsored by the Children's Oncology Group and using IC as a treatment for children with refractory or recurrent neuroblastoma showed immune activation as evidenced by elevated serum levels

*Department of Human Oncology, University of Wisconsin, Madison, WI 53705; †Paul P. Carbone Comprehensive Cancer Center, University of Wisconsin, Madison, WI 53705; ‡Department of Pathology and Laboratory Medicine, University of Wisconsin, Madison, WI 53705; §Department of Biostatistics and Medical Informatics, University of Wisconsin, Madison, WI 53705; ¶Department of Immunology, The Scripps Research Institute, La Jolla, CA 92037; ‖Provenance Biopharmaceuticals Corp., Waltham, MA 02451; and #Department of Pediatrics, University of Wisconsin, Madison, WI 53705

[1]R.K.Y. and N.A.K. are co-senior authors.

Received for publication March 27, 2012. Accepted for publication July 5, 2012.

This work was supported by National Institutes of Health Grants CA032685, CA87025, CA14520, and GM067386; Department of Defense Grant W81XWH-08-1-0559; grants from the Midwest Athletes for Childhood Cancer Fund, The Crawdaddy Foundation, and The Evan Dunbar Foundation; and University of Wisconsin-Madison Institute for Clinical and Translational Research Training Grant 1TL1RR025013-01.

Address correspondence and reprint requests to Prof. Paul M. Sondel, Immunology and Immunotherapy Program, University of Wisconsin-Madison, 4159 Wisconsin Institute for Medical Research, 1111 Highland Avenue, Madison, WI 53705. E-mail address: pmsondel@humonc.wisc.edu

Abbreviations used in this article: EpCAM, epithelial cell adhesion molecule; IC, hu14.18–IL-2; IHC, immunohistochemistry; IT, intratumoral(ly); IT-IC, intratumoral hu14.18–IL-2; IT-KS, intratumoral huKS–IL-2; i.v.-IC, i.v. hu14.18–IL-2; MFI, mean fluorescence intensity; TIL, tumor-infiltrating lymphocyte; TLNC, total live nucleated cell.

Freely available online through *The Journal of Immunology* Author Choice option.

www.jimmunol.org/cgi/doi/10.4049/jimmunol.1200934

of soluble IL-2Rα and lymphocytosis (7). The maximal tolerated dose was 12 mg/m^2/d when administered i.v. over 4 h for three consecutive days. This study showed that IC could be administered safely in pediatric patients at doses that induce immune activation. Subsequently, a phase II study through the Children's Oncology Group showed that recurrent neuroblastoma patients with nonbulky disease (evaluable only by sensitive [^{123}I]-meta-iodobenzylguanidine scintigraphy or bone marrow histology) treated with IC i.v. at 12 mg/m^2/d for 3 d every 4 wk had a 21.7% (5 of 23) complete response rate (8). These five patients had complete response status lasting 9, 13, 20, 30, and 35+ months. In contrast, patients with bulky disease (measurable by standard radiographic criteria) showed 0 of 13 responses. This study showed that IC warrants further testing in children with nonbulky high-risk neuroblastoma.

IC was also tested in adult melanoma patients. A phase I clinical trial of IC in patients with metastatic melanoma showed immune activation as measured by lymphocytosis, increased peripheral blood NK activity, and increased serum levels of the soluble IL-2Rα with reversible clinical toxicities at a maximum tolerated dose of 7.5 mg/m^2/d (9). In addition, 8 of 33 (24%) patients had stable disease after two courses of therapy. A separate phase I/II study of IC in patients with stage IV unresectable, cutaneous metastatic melanoma showed systemic immune activation as demonstrated by increases in serum levels of soluble IL-2R, IL-10, and neopterin, as well as increased tumor infiltration by T cells in postdosing biopsies (10). Stable disease was seen in two of nine (22%) patients treated with 4 mg/m^2/d of IC given as a 4-h i.v. infusion on three consecutive days every 4 wk. These two patients had stable disease status after courses 2 or 4, which progressed 4 mo later.

Localized versus systemic administration of immunocytokines was tested directly in tumor-bearing mice and showed an advantage for intratumoral (IT) administration of immunocytokines over i.v. administration. In an SCID mouse model using human melanoma xenografts and infused human PBLs, the therapeutic effects of immunocytokines consisting of an anti-EGFR mAb linked to IL-2 fusion protein or to TNF showed improved antitumor effects when administered IT compared with i.v. (11). IT injection of intact immunocytokine resulted in a survival advantage compared with IT injection of the mAb and IL-2 as separate IT injections. Survival time was prolonged by the IT application of fusion protein. In mice bearing s.c. Lewis lung carcinomas transfected with EpCAM, IT injection of huKS–IL-12/IL-2 (huKS1/4 mAb linked to a cytokine combination of IL-2 and IL-12) resulted in complete resolution of tumor (12). In an s.c. GD2$^+$ NXS2 neuroblastoma mouse model, intratumoral hu14.18–IL-2 (IT-IC) treatment resulted in a greater antitumor response compared with i.v. hu14.18–IL-2 (i.v.-IC) injection. This response was Ag specific, dose dependent, and greater than IT injection of IL-2 alone (13). The increased activity of IT-IC compared with i.v.-IC in NXS2 tumors was seen even in the absence of T cells (13). Clinical administration of IT IL-2 in melanoma patients showed local antitumor effects (14, 15). Because these clinical studies show local benefit of IT IL-2 in melanoma patients, and these preclinical studies show that IT-IC is more effective than IT IL-2 in tumor-bearing mice, clinical testing of IT-IC in melanoma patients with measureable disease appears to be warranted.

The mechanisms involved in improved antitumor effects seen with IT-IC administration are not clear. To evaluate the antitumor mechanisms of IT-IC and focus on the degree of leukocyte infiltration, we evaluated the effects of IT-IC in A/J mice bearing established GD2$^+$ NXS2 neuroblastoma. We hypothesize that IT-IC administration results in increased and sustained levels of IC in the tumor, augmenting infiltration of immune effector cells into the tumor and, thereby, enhancing the antitumor response. We developed methods to evaluate these hypotheses in tumor-bearing mice and demonstrate prolonged IC retention at tumor and augmented numbers of activated T and NK cells in tumor-infiltrating lymphocytes (TILs). To model patterns of infiltrating leukocytes in tumors of patients receiving IC in clinical trials, we developed a histological method in a preclinical mouse model to identify and quantify these infiltrating immune cells. Additionally, we used multicolor flow cytometry to quantify the expression of the killing ligand NKG2D on NK cells and CTLs, as well as to analyze the profile of IC and TILs at the tumor site following IT versus i.v. delivery of IC.

Materials and Methods

Mice

We obtained 7–8-wk-old female A/J mice from The Jackson Laboratory (Bar Harbor, ME). All mice were housed in university-approved facilities and were handled according to National Institutes of Health and University of Wisconsin-Madison Research Animal Resource Center guidelines.

Cell lines

NXS2 is a moderately immunogenic, highly metastatic, murine neuroblastoma hybrid cell line that was created as previously described (2). Briefly, hybridization of the GD2$^-$ C1300 murine neuroblastoma cell line (A/J background) with murine dorsal root ganglional cells from C57BL/6J mice was used to create the murine NX31T28 cell line. The NXS2 subline was generated by the selection of NX31T28 cells with high GD2 expression. NXS2 cells are of A/J background, that is, H2K^k positive/H2K^b negative MHC class I haplotype (2). The murine NXS2 cell line was grown in DMEM (Mediatech, Herndon, VA) supplemented with penicillin (100 U/ml), streptomycin (100 μg/ml), L-glutamine (2 mM; Life Technologies, Grand Island, NY), and 10% heat-inactivated FCS (Sigma, St. Louis, MO). Cells were maintained at 37°C in a humidified 5% CO_2 atmosphere.

ICs and immunotherapy

Humanized IC (APN301; Apeiron Biologics, Vienna, Austria) was supplied by the National Cancer Institute Biologics Resources Branch (Frederick, MD) via a collaborative relationship with Merck KGaA (Darmstadt, Germany). IC is an immunocytokine consisting of intact human IL-2 genetically linked to the C-termini of each human IgG1 H chain of the hu14.18 mAb (1). The humanized huKS–IL-2 immunocytokine (EMD273066) was generated and provided by EMD-Lexigen Research Center (Billerica, MA).

Tumor models

Well-established tumor model. A/J mice were injected s.c. with 2 × 10^6 cells of NXS2 murine neuroblastoma in 100 μl PBS in the lower right quadrant of the abdomen. Tumors were allowed to grow until the average volume was 30–150 mm^3 (volume measured with mechanical calipers = width × width × length/2); normally, this required 14–18 d. Mice were then randomized into appropriate treatment groups and received 50 μg IC treatment daily for three consecutive days (either i.v. or IT). Mice were given i.v.-IC by tail vein injection in 100 μl PBS. IT injections consisted of IC in 100 μl PBS, delivered into the s.c. tumor with a 30-gauge needle. Control treatments consisted of an equivalent volume of PBS administered by IT injection.

Early established two-tumor model. A/J mice were injected s.c. with 2 × 10^6 cells of NXS2 murine neuroblastoma in 100 μl PBS on day 0 in the lower right quadrant of the abdomen to establish an initial (primary) tumor. After 4 d, mice were injected again s.c. with 2 × 10^6 cells of NXS2 murine neuroblastoma in 100 μl PBS in the lower left quadrant of the abdomen to establish a second (distant) tumor. Mice were randomized on day 4 (immediately prior to depletion Ab injections and second tumor implantation) into appropriate treatment groups and received 15 μg IC treatment daily for five consecutive days (days 7–11). Mice were given i.v.-IC by tail vein injection in 100 μl PBS. IT injections consisted of IC in 100 μl PBS placed into the primary tumor with a needle. IT treatment was only provided to the primary (local) tumor. Control treatments consisted of an equivalent volume of PBS administered by i.v. or IT injection. Tumor volumes of the initial (local) and secondary (distant) tumors were measured using mechanical calipers (volume = width × width × length/2).

End points for progressive tumor growth

The end point of all tumor growth and survival studies was death of the animal or excessive tumor burden, as determined by both tumor size (15 mm in any direction) and the condition and behavior of the animal. These criteria

are provided in the University of Wisconsin-Madison Research Animal Resource Center guidelines. The decision to euthanize an animal was made by an independent observer without regard for treatment group.

Cell-depletion regimens

Local and distant tumors were induced according to the early established tumor model. To deplete NK cells, mice were injected i.p. with 1.6 mg anti-asialo GM1 Ab (Wako Chemicals, Richmond, VA) or 1.6 mg rabbit IgG isotype control (Sigma) in a total volume of 200 μl PBS on days 4, 9, and 16. To deplete T cells, mice were injected i.p. with mixtures of anti-CD4 and anti-CD8 mAbs (250 μg of each) or 500 μg rat IgG (Sigma) isotype control in a total volume of 200 μl PBS on days 4, 9, and 16. Mice received five daily IT injections (days 7–11) of 15 μg IC to the primary tumor in a volume of 50 μl PBS or 50 μl control PBS. Tumor volumes were measured using mechanical calipers.

IC-retention experiments

Tumors were induced according to the well-established tumor model and then randomized to receive a single treatment of IT-IC (IT injection of 50 μg IC in 100 μl PBS), i.v.-IC (i.v. injection of 50 μg IC in 100 μl PBS), or intratumoral huKS–IL-2 (IT-KS) (IT injection of 50 μg huKS–IL-2 in 100 μl PBS). Mice were sacrificed at various times after treatment, and their tumors were resected for flow cytometry.

Histology experiments and immunohistochemistry

Mice treated according to the well-established tumor model were sacrificed 48 h after treatment completion, and their tumors were resected for histology. The tumors were embedded in OCT, flash frozen in liquid nitrogen, and stained. Briefly, frozen sections were cut onto slides using a cryostat, fixed in cold acetone, and dried. After rehydration, sections were blocked with 5% rabbit serum (Sigma) for 25 min, washed, and incubated with optimally titered mAb (rat anti-mouse CD45 [clone 30-F11], CD3 [clone 17A2], CD4 [clone GK1.5], CD8 [clone 53-6.7], F4/80 [clone BM8], and NKG2A/C/E [clone 20d5; all from eBioscience]) overnight in 1% rabbit serum. Following a wash, a biotinylated rabbit anti-rat secondary Ab was applied for 90 min, followed by an avidin-biotin complex (ABC kit; Vector Laboratories, Burlingame, CA). Slides were developed with DAB (Vector Laboratories) for 4.5 min, counterstained with Mayer's hematoxylin (Sigma) for 90 s, washed in running tap water for 5 min, and mounted.

Quantitation of immunohistochemistry

A histological method was developed to identify and quantify leukocyte infiltration patterns in these IT-IC–treated tumors. Digital pictures of the stained sections were taken at low magnification (×10), and quantitative analysis was performed using ImageJ software (National Institutes of Health). The digital photographs were placed on reproducible grids, and five representative areas of the same size within each frozen section were chosen. These five subsamples were inspected visually so that positive and negative cells could be manually counted within each subsample. Analogous grids and subsamples of the same size were obtained for each individual frozen section specimen being analyzed. This manual counting was done, using a blinded system, by two individuals. These results were confirmed by a board-certified hematopathologist who assessed the methods and analyses (E.A.R.). Percentages of subsamples were averaged within a sample, and significance tests were performed using Prism 5 (version 5.0.4) software (GraphPad).

Flow cytometry

Tumors were established and mice were treated according to the well-established tumor model. Forty-eight hours after treatment completion, mice were sacrificed, and their tumors and spleens were resected for flow cytometry. Single-cell suspensions were made by disassociating the tissues through brass mesh (30 openings/inch) and then 50-μm nylon filters. Cell counts were determined using a Beckman Coulter cell counter or hemacytometer. About 1 million cells were stained with the following Abs at 4°C for 30 min: FITC-conjugated anti-mouse NKG2A/C/E (clone 20d5; eBioscience), PE-conjugated anti-mouse NKG2D (clone CX5; eBioscience), PE-Cy5–conjugated anti-mouse F4/80 (clone BM8; BioLegend), PerCP-eFluor 710–conjugated anti-mouse F4/80 (clone BM8; eBioscience), PE-Cy7–conjugated anti-mouse CD4 (clone GK1.5; eBioscience), allophycocyanin-conjugated anti-mouse CD3e (clone 145-2C11; BioLegend), Alexa Fluor 700-conjugated anti-mouse CD45 (clone 30-F11; BioLegend), allophycocyanin-eFluor 780–conjugated anti-mouse CD8a (clone 53-6.7; eBioscience), CD16/32 Fc Block (clone 93; BioLegend), PE-conjugated goat anti-human IL-2 (clone MQ1-17H12; eBioscience), and PE-conjugated goat anti-human IgG Fcγ (cat. 12-4998-82; eBioscience). Cells were washed and analyzed using the Becton Dickinson LSRII flow cytometer. Analyses of data were performed using FlowJo software. Fluorochromes Minus Ones were used to distinguish positively stained populations. Erythrocytes were subtracted from the denominator to allow analyses to focus only on nucleated cells. Results are reported as the percentage of positive cells or as mean fluorescence intensity (MFI) units. To obtain total live nucleated cells (TLNCs) or $CD45^+$ cells, we first gated on cells using forward and side scatter, then on single cells ("singlets") using forward scatter width, then on live cells using DAPI, and then on $CD45^+$ cells to get tumor-infiltrating leukocytes and on $CD45^-$ cells to get tumor and stromal cells. TLNCs were obtained by the addition of $DAPI^-$ $CD45^-$ cells and $CD45^+$ cells.

Statistical methods

One- or two-tailed (if there was no a priori hypothesis) Student *t* tests under the normality assumption were used to determine significance of differences in antitumor responses (tumor volume, tumor infiltration, tumor growth inhibition, and delivery and retention of IC) between experimental and relevant control groups. Survival curves were generated using the Kaplan–Meier method and statistically compared using the Log-Rank (Mantel–Cox) proportional hazard test. Data are presented as mean ± SEM; p values < 0.05 were considered statistically significant. Because of the exploratory nature of these analyses, multiplicity adjustments were not made. Graphs were generated and significance tests were performed using GraphPad Prism 5 (version 5.04) software.

Results

IT-IC treatment results in enhanced inhibition of tumor growth and augmented survival compared with controls

Using the well-established tumor model, we established the antitumor effects of IT-IC compared with the no-treatment and IT PBS control groups. IT-IC treatment induced greater inhibition of tumor growth than did no treatment or IT PBS (Fig. 1A). IT-IC also resulted in improved survival compared with the controls (Fig. 1B). Although the change in growth induced by IT-IC is seen quickly (48 h after the last IT-IC treatment) in Fig. 1A, histological evaluation confirms an immunotherapeutic effect. H&E stains of IT-IC–treated tumors showed increased lymphocyte infiltration, greater cell death, and increased necrosis compared with no-treatment controls (Fig. 1C, 1D) and IT PBS controls (data not shown).

Tumors treated with IT-IC are characterized by increased NK and T cells

Frozen sections of tumors were stained for various cell-specific surface markers. Fig. 2 shows representative samples of an NXS2 tumor treated with localized IC and stained with an Ab specific for the CTL marker CD8a. There was a visually striking increase in the amount of infiltrating CTLs compared with the control tumor treated with IT PBS (Fig. 2A versus Fig. 2B). Representative samples of an NXS2 tumor treated with localized IC and stained with an Ab specific for NKG2A/C/E, a marker of mouse NK cells, also showed a striking increase in the amount of infiltrating NK cells compared with tumors treated with IT PBS (Fig. 2C versus Fig. 2D). We developed a histological method to quantify and characterize the augmented TILs seen in these IT-IC–treated tumors.

Digital photographs of these stained sections were taken at low magnification (×10), and quantitative analysis was performed using ImageJ software. The digital photographs were placed on reproducible grids, and five representative areas of the same size within each frozen section were used to manually count positive and negative cells within each subsample. Percentages of subsamples were averaged within a sample, and significance tests were performed using GraphPad Prism 5 software.

By this method, IT-IC–treated tumors showed higher tumor leukocyte infiltration compared with the controls. An overall increase in leukocyte infiltration was demonstrated by an increase in $CD45^+$ cells in the IT-IC–treated tumors (Fig. 2E). These treated

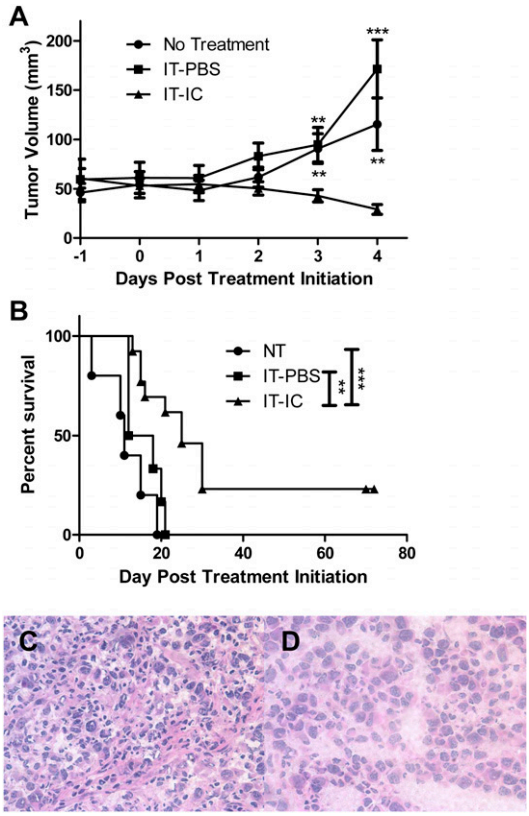

FIGURE 1. IT-IC shows enhanced antitumor effects compared with control treatments. Tumors were established according to the well-established tumor model. (**A**) Tumor growth curves of IT-IC–treated ($n = 12$), IT PBS-treated ($n = 12$), and untreated ($n = 8$) s.c. NXS2 tumor in A/J mice. Data were obtained from two independent experiments. (**B**) Kaplan–Meier survival curves of IT-IC–treated ($n = 13$), IT PBS-treated ($n = 6$), and untreated ($n = 5$) mice. Data represent three independent experiments. (**C**) H&E stain of IT-IC–treated NXS2 tumor 4 d posttreatment initiation. Original magnification ×40. (**D**) H&E stain of untreated NXS2 tumor. Original magnification ×40.

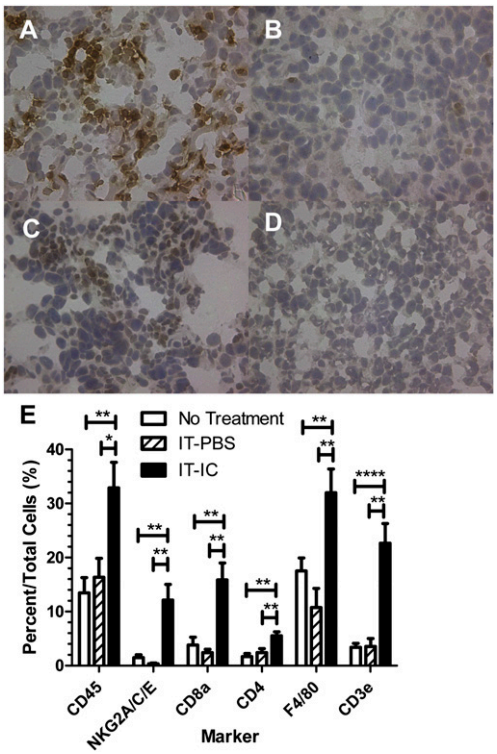

FIGURE 2. IT-IC is distinguished by increased TILs. Representative IHC stains of s.c. NXS2 tumor frozen sections were photographed. Sections were stained with either anti-CD8a (**A**, **B**) or anti-NKG2A/C/E (**C**, **D**) Abs. Sections from either IT-IC–treated tumors (A, C) or untreated tumors (B, D) are shown. Original magnification ×40. (**E**) Quantification of IHC photographs using the manual counting method. IT-IC–treated ($n = 20$) tumors are characterized by higher tumor leukocyte infiltration percentages ($CD45^+$, $CD3^+$, $CD8a^+$, $NKG2A^+$, $F4/80^+$) than are IT PBS-treated ($n = 10$) and untreated ($n = 15$) tumors. Data were obtained from three independent experiments. $^*p < 0.05$, $^{**}p < 0.01$, $^{****}p < 0.0001$.

tumors also had increased numbers of T cells and macrophages, as shown by increases in $CD3^+$, $CD4^+$, $CD8a^+$ cells and $F4/80^+$ cells, respectively (Fig. 2E). An increased frequency of cells bearing the NKG2A receptor was also seen in the IT-IC–treated tumors; these $NKG2A^+$ cells are presumably licensed NK cells and/or activated cytotoxic T cells (Fig. 2E) (16, 17). These data were later confirmed by flow cytometry (see below).

T cells and NK cells are involved in the antitumor effects of IT-IC against local and distant tumors

We wanted to determine whether these TILs were involved in the observed antitumor effects of IT-IC. In this series of experiments, tumor-bearing mice were depleted of $CD4^+/CD8a^+$ T cells or NK cells (asialo $GM1^+$) or double depleted of $CD4^+/CD8a^+$ T cells and NK cells. The early established two-tumor mouse model was used for these depletion studies to evaluate the antitumor effects of IT-IC on the local primary (injected) and distant secondary (noninjected) tumor. The early established model enables IC treatment to begin when tumors are smaller, enabling this immunotherapy to have greater measurable antitumor effects; this is in contrast to the well-established tumor model (as used in Fig. 1), in which larger tumors are needed to be able to collect tumor 48 h after treatment for flow cytometry and histology studies. IT-IC treatment was given only to the local (primary) tumor, and tumor sizes of both the local and distant tumors were measured.

Fig. 3A shows that IT-IC induced marked inhibition of growth of the local tumor compared with IT PBS. The antitumor effect of IT-IC on the local tumor was nearly abrogated by the T cell depletion. In addition, NK cell depletion caused substantial inhibition of the antitumor effects of IT-IC on the local tumor. Thus, both T and NK cells are involved in the antitumor effects of IT-IC against the local tumor in this model. Fig. 3B shows that, in the absence of T or NK depletion, administration of IT-IC to the local tumor dramatically inhibits the growth of the distant (noninjected) tumor (compared with the growth of the distant tumor in mice that received IT PBS). Fig. 3B shows that NK cell depletion, as well as T cell depletion, causes virtual abrogation of the IT-IC antitumor effect on the distant tumor, suggesting that local IT-IC treatment of the primary tumor results in systemic immune activation, causing antitumor effects at the distant tumor site.

Data show reduced survival of IT-IC–treated mice when either NK or T cells are depleted (Fig. 3C) in this early established tumor model. Depletion of T cells or NK cells in IT-IC–treated mice resulted in no long-term survivors compared with IT-IC–treated mice without depletion, which had 62.5% (10 of 16) long-term, tumor-free survivors. These 10 tumor-free mice were rechallenged by s.c. injection of 2 million NXS2 cells ~110 d after implantation of their initial local primary tumor. Ninety percent of the rechallenged mice (9 of 10) rejected the tumor rechallenge and remained tumor-free. This result suggests that mice rendered tumor-free by IT-IC treatment developed long-term memory T cell immunity to

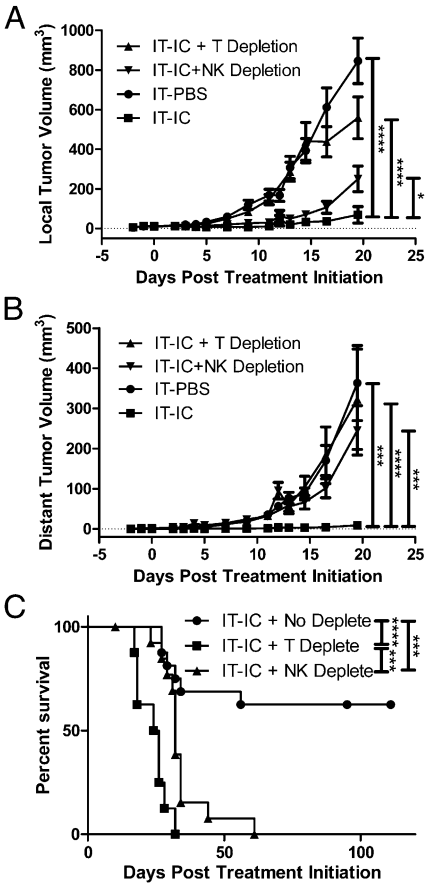

FIGURE 3. T cell and NK cell depletion reduces IT-IC–induced antitumor effects. Tumors were established according to the early-established tumor model. Local tumor (**A**) and distant tumor (**B**) growth curves of IT-IC–treated T cell-depleted mice (▲, $n = 8$), IT-IC–treated NK cell-depleted mice (▼, $n = 16$), IT-IC–treated mice without depletion (■, $n = 16$), and IT PBS-treated mice (●, $n = 16$) bearing s.c. NXS2 tumors. (**C**) Kaplan–Meier survival curves of mice with the early established two-tumor NXS2 model, shown in (A) and (B) for groups receiving IT-IC treatment, with and without NK or T cell depletion. Data were obtained from two independent experiments. $*p < 0.05$, $***p < 0.001$, $****p < 0.0001$.

NXS2, as shown previously for mice with early tumors made tumor free by the combination of i.v.-IC and IL-2 treatment (18).

IT-IC treatment results in better inhibition of tumor growth and enhancement of survival compared with i.v.-IC treatment

We hypothesized that local injection of IC will induce better antitumor effects than will systemic injection. Therefore, the antitumor effects of IT-IC were compared with those of i.v.-IC. Mice bearing a single established s.c. NXS2 tumor were treated with IT-IC or i.v.-IC beginning on day 0. Inhibition of tumor growth was more striking in IT-IC–treated mice compared with i.v.-IC–treated mice (Fig. 4A). IT-IC–treated mice also demonstrated improved survival compared with i.v.-IC–treated mice (Fig. 4B).

IT-IC treatment is characterized by higher percentage of NKG2A/C/E$^+$ cells and a lower percentage of living tumor cells in the tumor than seen following i.v.-IC treatment

IT-IC treatment induced greater inhibition of tumor growth compared with i.v.-IC treatment (Fig. 4A). IT-IC also resulted in improved survival compared with i.v.-IC (Fig. 4B). As a result, we wanted to compare the TILs of IT-IC–treated mice with those of i.v.-IC–treated mice. Tumors of treated mice (and untreated control mice) were harvested 48 h after the last IC treatment, frozen, sectioned, and histologically stained for various cell-specific surface markers (Fig. 4C) or resected, disaggregated, filtered, and stained with fluorescent Abs for analysis by flow cytometry (Fig. 4D). The immunohistochemistry (IHC) analyses showed that IT-IC and i.v.-IC caused significant increases in NK cells, CD3 cells, and CD8 cells (Fig. 4C). These increases in NK cells and CD8 cells after IC treatment were confirmed by flow cytometry (Fig. 4D). In addition, the flow cytometry analyses showed that tumors from IT-IC–treated mice had a higher percentage of NKG2A/C/E$^+$ cells and CD8a$^+$ cells (measured as a percentage of total viable nucleated cells) compared with tumors from i.v.-IC–treated mice (Fig. 4D). Tumors from IT-IC–treated mice also had a higher percentage of F4/80 macrophages compared with untreated mice (Fig. 4D). This "increase" in the percentage of macrophages is relative to all other cells in the tumor; because the IT-IC–treated tumors are smaller than the untreated tumors, the increased percentage of macrophages (relative to TLNCs remaining in the tumor) likely corresponds to an actual decrease in the actual numbers of macrophages. This is even more clear when macrophages are evaluated as a percentage of tumor-infiltrating leukocytes (CD45$^+$ cells) (Fig. 4E). For these calculations in Fig. 4D, erythrocytes were subtracted from the total viable cells to account for recovered viable nucleated cells. We then analyzed (Fig. 4E) the presence of these leukocyte populations as a percentage of TILs (CD45$^+$ cells), rather than as a percentage of total viable nucleated cells, including tumor cells. IT-IC resulted in a significant decrease in the percentage of CD4$^+$ T cells in the TIL population compared with i.v.-IC or no treatment. Both i.v.-IC and IT-IC caused increases in the percentage of NK cells (as detected by NKp46 and NKG2A/C/E) and CTLs (CD8a$^+$). Both i.v.-IC and IT-IC treatment resulted in some detectable decreases in the percentage of macrophages (F4/80$^+$) (Fig. 4E) in these tumors compared with the percentage of macrophages in the untreated tumors. This "decrease" in the percentage of macrophages is relative to all leukocytes and reflects the fact that the tumors have decreased in size with IT-IC treatment and have an increase in the percentage of CD45$^+$ cells (per total live cells, as seen in Fig. 4D). The fact that the percentage of macrophages increased less prominently than did CD8 cells or NK cells relative to TLNCs (Fig. 4D) explains why the macrophages (as a percentage of CD45$^+$ cells) decrease in Fig. 4E, whereas the CD8 and NK cells increase (Fig. 4D) with IT-IC treatment. The percentage of NKG2A/C/E$^+$ cells was significantly higher for IT-IC than for i.v.-IC (Fig. 4E). These flow cytometry studies also showed that IT-IC–treated tumors have lower percentages of living tumor cells than do i.v.-IC–treated tumors (Fig. 4F), consistent with the tumor growth and survival data summarized above (Fig. 4A, 4B).

IT-IC treatment induces a greater increase in NKG2A/C/E$^+$ and NKG2D$^+$ T and NK cells locally than systemically

Our depletion studies showed that both NK cells and T cells are involved in the antitumor effects of IT-IC (Fig. 3). Similarly, the IHC and flow cytometry studies showed increases in NK and CD8 cells in IT-IC–treated tumors (Fig. 4C–E). We evaluated the phenotypes of these NK and CD8 cells in TILs and compared them with NK and CD8 cells found in the spleen. We characterized the presence of NKG2A/C/E$^+$ cells, shown to be necessary for self recognition (19), within the separate populations of NK cells (NKp46$^+$, Fig. 5A) and cytotoxic T cells (CD8a$^+$, Fig. 5B). The level of NKp46$^+$ cells that coexpress NKG2A/C/E in untreated mice was similar in the tumor and in the spleen (Fig. 5A). Tumors treated with IT-IC or i.v.-IC had an increase in the proportion of NKp46$^+$ cells that coexpress NKG2A/C/E (Fig. 5A). A statistically sig-

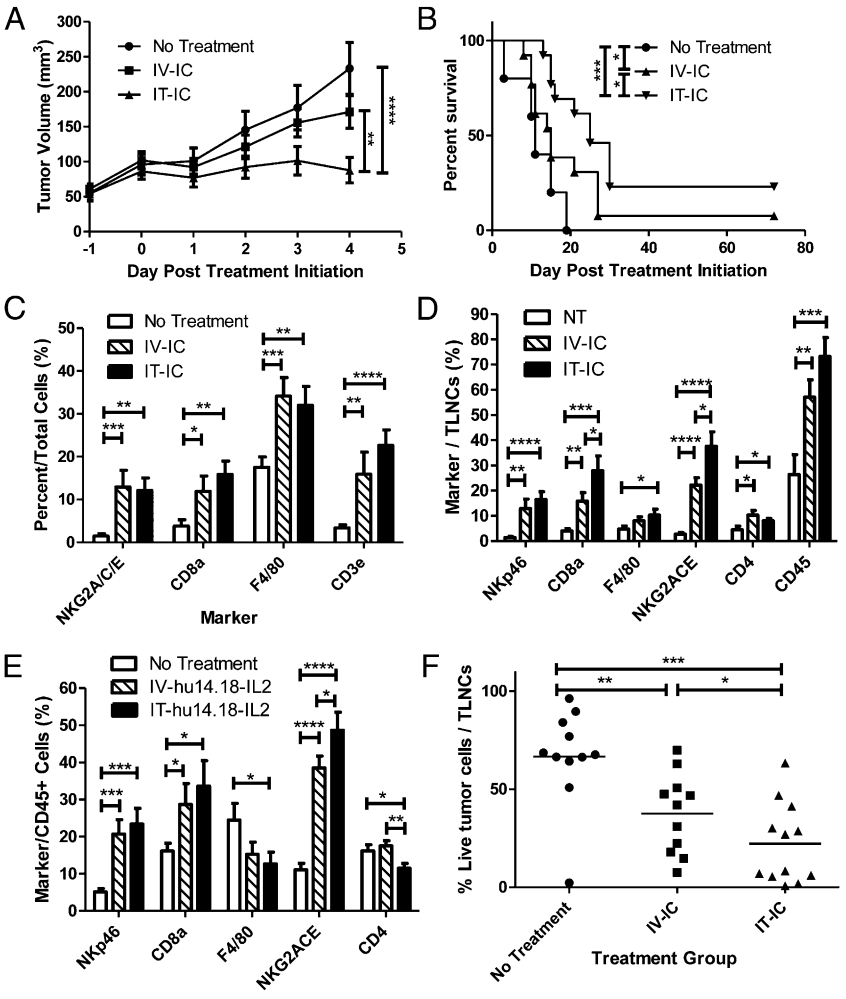

FIGURE 4. IT-IC is more effective than i.v.-IC in slowing tumor growth and prolonging survival. Tumors were established according to the well-established tumor model. Mice given IT-IC, i.v.-IC, or no treatment were followed. Tumor growth curves (n = 30/group, four independent experiments) (**A**) and Kaplan–Meier survival curves (n = 13/group, three independent experiments) (**B**) are plotted. Mice in these treatment groups were also sacrificed for characterization of the TILs, using both manual blinded counting of IHC photographs (n = 15/group, three independent experiments) (**C**), as well as flow cytometric analyses (**D**). (**E**) Populations of TILs as a percentage of total leukocytes within a tumor ($CD45^+$). (**F**) Populations of live NXS2 tumor cells as a percentage of TLNCs within a tumor. (D–F: n = 11/group, three independent experiments). $*p < 0.05$, $**p < 0.01$, $***p < 0.001$, $****p < 0.0001$.

nificant difference was not found in the augmented coexpression of NKG2A/C/E with IT-IC versus i.v.-IC. A similar effect was seen in the spleen. IT-IC and i.v.-IC treatment both induced similar augmented coexpression (over that seen in untreated mice) of NKG2A/C/E on $NKp46^+$ spleen cells (Fig. 5A); the frequencies of the NKG2A/C/E phenotype on $NKp46^+$ cells in spleens are comparable to those seen in TILs. In contrast, when examining $CD8^+$ cells for coexpression of NKG2A/C/E, the data in Fig. 5B demonstrate that, even without treatment, the percentage of CD8 cells that coexpress NKG2A/C/E is far greater in the TIL population than in the spleen. In TILs and spleens, both IT-IC and i.v.-IC treatment induced significant increases in the percentages of CD8 cells that coexpress NKG2A/C/E over that seen in untreated mice. However, the percentages seen in TILs are 10–15-fold greater than those seen in the spleen. We further examined these NK and CD8 cells that coexpress NKG2A/C/E for the level of their surface expression of the NKG2D effector receptor (Fig. 5C, 5D). We found that tumors treated with i.v.-IC or IT-IC had significantly higher expression levels (MFI) of $NKG2D^+$ on $NKp46^+$ $NKG2A/C/E^+$-coexpressing NK cells than did control mice (Fig. 5C). In contrast, these increases in NKG2D MFI were not seen in the comparable populations in the spleen (Fig. 5C). Similar analyses were done for NKG2D expression on the cells coexpressing CD8 and NKG2A/C/E (Fig. 5D). As in Fig. 5C, the MFI of NKG2D in the $CD8^+$ TIL population was augmented by IT-IC and by i.v.-IC. The level of NKG2D augmentation on these $CD8^+$ TILs after IC treatment was not statistically significant for IT versus i.v. delivery ($p = 0.107$). These MFI levels of NKG2D in the $CD8^+/NKG2A/C/E^+$ TIL populations were significantly higher than were the MFI levels of NKG2D seen in the comparable splenic populations (Fig. 5D). We examined expressivity of NKG2D ligands on NXS2 and found a large increase in RAE-1γ expression on tumor cells obtained from NXS2 cells harvested from tumors growing in vivo (data not shown).

IT-IC treatment results in augmented delivery and retention of IC in the tumor compared with i.v.-IC

We next compared the delivery and retention of IC in tumor tissue following IT-IC and i.v.-IC treatment. Tumors were resected from i.v.-IC– or IT-IC–treated mice at various time points posttreatment, disaggregated, filtered, and stained with fluorescently labeled anti-human Fcγ-chain or anti-human IL-2 (as two separate ways to detect IC still bound to the NXS2) for analysis by flow cytometry. To compare the effect of the GD2-specific IC in these studies to the delivery and retention of a nonspecific immunocytokine that could not bind specifically to the $GD2^+$ NXS2 tumor, we also evaluated animals that received IT administration of the KS–IL-2, which consists of IL-2 linked to an mAb that recognizes the EpCAM and does not recognize GD2 (and, thus, is not able to specifically recognize the $EpCAM^-$ NXS2 tumor). Because absolute MFI values are not consistent from day to day, data collected in these experiments were normalized to the MFI values for our negative control, the IT-KS–IL-2 group. By doing this, Fig. 6 shows the fold change of IC present on tumor cells after IT or i.v. treatment compared with IT-KS–IL-2. IT-IC and i.v.-IC both had fold changes > 1, indicating that the GD2-specific IC localizes

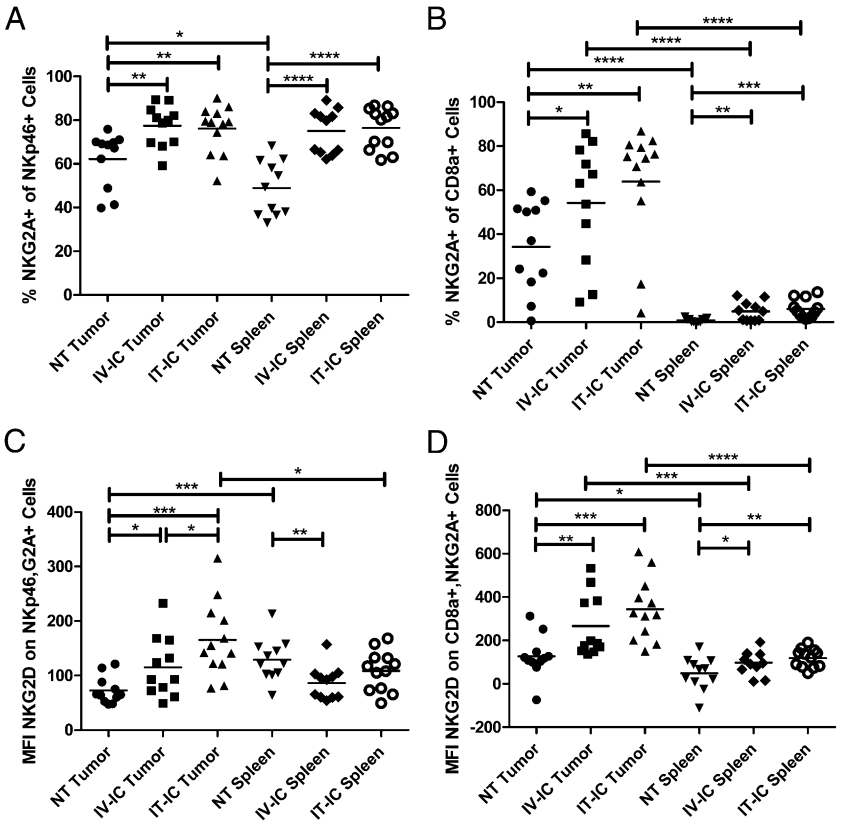

FIGURE 5. Treatment with IC increases NKG2A/C/E$^+$ NK and T cells in tumor and spleen and increases NKG2D expression within tumors. Flow cytometric analyses show percentages of NKG2A/C/E$^+$ cells within the NKp46$^+$ NK cell populations (**A**) and the CD8a$^+$ cytotoxic T cell populations (**B**) within tumors and spleens. Flow cytometric analyses of NKG2D expression on NKp46$^+$/NKG2A/C/E$^+$ NK cell populations (**C**) and the CD8a$^+$/NKG2A/C/E$^+$ cytotoxic T cell populations (**D**) within tumors and spleens. All data represent three independent experiments (n = 11 mice/group). *$p < 0.05$, **$p < 0.01$, ***$p < 0.001$, ****$p < 0.0001$.

more effectively to the NXS2$^+$ tumor compared with the nonspecific immunocytokine, KS–IL-2; furthermore, because the NXS2 tumor is GD2$^+$ but does not have IL-2Rs, the specific IC would be expected to localize better to NXS2 than would the nonspecific KS–IL-2 or unconjugated free IL-2.

There were ~65-fold (Fig. 6A) and ~150-fold (Fig. 6B) increases in the amount of IC detected on tumor cells after treatment with IT-IC compared with treatment with i.v.-IC when detecting IC with the anti-Fcγ Ab and anti–IL-2 Ab (Fig. 6), respectively, 15 min posttreatment. This indicates that initially after treatment, local IC administration results in far more IC being present at the tumor site than does systemic i.v. administration. Fig. 6 shows that in the 75 h after IT or i.v. injection, the IC level detected in the tumor (after IT-IC treatment) plateaus between 4 and 6 h, with lower levels detected at 27 and 75 h. There is substantially more area under the curve when IC is given IT compared with i.v. At 27 and 75 h posttreatment, there was no difference in tumor IC concentration between IT- and i.v.-treated mice.

Interestingly, Fig. 6A (Fcγ) and Fig. 6B (IL-2) show that IC administered systemically (i.v.) takes some time to reach the tumor site. At 15 min and 1 h post–i.v.-IC treatment, the same amount of IC is present on tumor cells as after the control IT-KS–IL-2 treatment (MFI ratio = 1). However, there is ~5-fold increase and 2-fold increase in IC at the 3.5-h time point (Fig. 6), using anti-Fcγ Ab or anti–IL-2 Ab, respectively. This is followed by an eventual decrease in IC at 75 h.

Discussion

Data presented in this article help to elucidate possible mechanisms of enhanced antitumor effects of localized IC therapy and assist in distinguishing the IT-IC antitumor effect from the i.v.-IC antitumor effect. In this study, we show that IT-IC treatment induces improved inhibition of tumor growth and augmented survival compared with no treatment or treatment with IT PBS. IHC and flow cytometric analyses show an increased percentage of NK and T cells in IT-IC–treated tumors. Depletion studies show that T cells and NK cells are involved in the antitumor effects of IT-IC on directly injected local tumors and on noninjected distant tumors in those same animals. Depletion of either immune cell population substantially attenuates the observed antitumor effects on both the local and distant tumors. These data suggest that both T cells and NK cells are necessary for the local and distant antitumor effects observed under these conditions. Although NK cells may exert a more direct and immediate effect (through Ab-dependent cellular cytotoxicity), and T cells may exert a more delayed effect through an adaptive immune response, we are not able to clarify these mechanisms from the data presented in this study. Furthermore, other possible mechanisms include direct induction of tumor apoptosis or disruption of the tumor microenvironment or tumor vascular system.

We also show that IT-IC treatment causes better tumor growth inhibition and survival than does i.v.-IC treatment, which is consistent with flow cytometry analyses demonstrating that IT-IC results in a lower percentage of living tumors cells compared with i.v.-IC treatment. Furthermore, flow cytometry analyses show that IT-IC treatment is characterized by a higher percentage of NKG2A/C/E$^+$ cells. IT and i.v. treatment with IC increases the fraction of NK cells and CD8 cells that express NKG2A/C/E, whereas IT-IC increases expression levels of the NKG2D effector receptor on NK and CD8 cells to a greater degree than does i.v.-IC. Finally, flow cytometry analyses were used to show that IT-IC treatment results in augmented delivery and retention of IC to tumor compared with i.v.-IC treatment.

Although immunocytokines allow the targeting of immune-stimulating cytokines directly to the tumor microenvironment, systemic administration is still limited by dose-limiting toxicities (7, 9). These dose-limiting toxicities are due to the systemic effects of the IL-2 component of the immunocytokine (i.e., fever, capillary

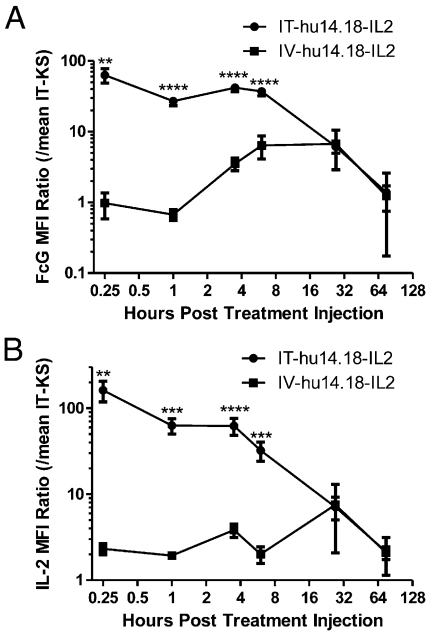

FIGURE 6. IT-IC treatment results in augmented IC localization and increased IC retention compared with i.v.-IC. Tumor-bearing mice given IC IT or i.v. were sacrificed at various times, and their tumors were disaggregated. (**A**) Flow cytometric measurements of levels of human IgG Fcγ Ab fragment on NXS2 tumor cells ex vivo at various times posttreatment. (**B**) Flow cytometric measurements of levels of human IL-2 on NXS2 tumor cells ex vivo at various times posttreatment. All MFI values are normalized to an IT nonspecific control immunocytokine (IT-KS–IL-2). Data represent three independent experiments with approximately six mice/group/time point. $^{**}p < 0.01$, $^{***}p < 0.001$, $^{****}p < 0.0001$.

leakage, and secondary effects of capillary leakage, such as hypotension) and effects from the mAb component of the immunocytokine; for IC, these include neuropathic pain due to mAb recognition of selective GD2-expressing peripheral nerves. Finding a strategy of IC administration that maximizes the direct delivery of IC to the tumor site and potentially decreases dose-limiting systemic toxicities would be clinically beneficial. Using the NXS2 model, we demonstrate a greater antitumor response with localized IC administration compared with an equivalent systemic IC dose in the treatment of established s.c. tumors. Importantly, IT-IC treatment increased delivery of IC to the tumor site; substantially higher levels of IC were found at the tumor site for several hours following IT-IC compared with i.v.-IC.

IT-IC resulted in complete resolution of both the directly treated local and noninjected distant tumors in several mice. Several mechanisms may result in the antitumor effects of both local and distant tumors: IT-IC may be circulating and having a systemic effect, IT-IC may be inducing a systemic immune response by the host's immune system, or a combination of both. We acknowledge that our experimental design may play some role in our observation that NK depletion (which begins on day 4, 4 d after implantation of the primary tumor and just prior to implantation of the secondary tumor) more potently interferes with the IC effects against the distant tumor than the primary one. We also know from previous studies that T cells from treated mice can respond to NXS2 in an Ag-dependent manner (18). Our results indicate that IT-IC induces a systemic immune response. T cells and NK cells were required for rejection of both primary and distant tumors, and 90% of mice that became tumor-free following IT-IC treatment were able to subsequently reject rechallenge with 2×10^6 NXS2 cells.

The IL-2 component of the IC augments the effects of the mAb and was shown to increase the number and activation state of NK cells, as well as to stimulate tumor cell killing by Ag-specific T cells (20). The IL-2 component can stimulate both NK and T cells via IL-2R, independent of Fc or TCR binding, respectively (1, 21–23). Using a metastatic model of NXS2 neuroblastoma metastasizing to bone marrow in A/J mice, i.v.-IC therapy was previously shown to be exclusively mediated by NK cells (2, 3). In contrast, our model investigates possible immune effector cells within well-established s.c. tumors and shows a necessary role for both NK and T cells in response to localized IT-IC therapy. There is an increased percentage of NKG2A$^+$ on CD8a$^+$ T cells, as well as increased NKG2D expression on CD8a$^+$/NKG2A$^+$ T cells in tumors versus spleens within similarly treated mice (Fig. 5B–D). This may suggest at least some inherent importance of T cells in combating tumor cells in this model because NKG2A/C/E$^+$ cells were shown to be necessary for self recognition (19). Furthermore, the statistically significant increase in NKG2D expression on NK cells after IT-IC versus i.v.-IC treatment (Fig. 5C) may reflect a mechanism that plays some part in the enhanced antitumor effect of IT versus i.v. IC treatment. In addition, the increased expression of NKG2D might be considered a marker of activation and suggests that other pathways (not assayed for in this study) might be further activated by IT-IC compared with i.v.-IC.

Depletion data from a two-tumor model showed that T cells, as well as NK cells, play a large role in the IT-IC antitumor effect compared with the previously shown NK-predominant cell-mediated i.v.-IC antitumor effect (3). Perhaps having substantial IL-2 bound to the surface of tumor cells after IT-IC treatment (Fig. 6B) is directly or indirectly responsible for increasing these specific lymphocytes (NKG2A/C/E$^+$ TIL) or altering their phenotype (increasing expression of NKG2D effector receptor) and enhancing the antitumor effect compared with i.v.-IC treatment. In vitro data suggest that immunocytokine on tumor cells enables cells with IL-2Rs to form more activated immune synapses with the tumor cells than they would using mAb in combination with IL-2 (24, 25). IT–IC-treated mice compared to i.v.–IC-treated mice show a small, but significant, increase in NKG2D expression on NKp46$^+$/NKG2A$^+$ double-positive cells, as well as a small, but nonsignificant, increase in NKG2D expression on CD8a$^+$/NKG2A$^+$ cells (Fig. 5C, 5D). This may indicate a phenotypic advantage of resulting TILs when treating with IT-IC. Expression of NKG2D on activated CD8$^+$ T cells was shown to account for TCR-independent cytotoxicity against malignant cells in vitro (26). Its enhanced expression on CD8$^+$ TILs, but not spleen cells, following i.v. or IT treatment with IC in our study demonstrates the localized activation of T cells, at the tumor site, induced by IC treatment. We examined expressivity of NKG2D ligands on NXS2 and found a large increase in RAE-1γ expression ex vivo (data not shown). Therefore, in addition to being a marker of activation, NKG2D may play a direct role in the enhanced antitumor effects.

Previous data showed therapeutic and safety benefits of localized versus systemic immunocytokine therapy in preclinical models (11–13), as well as localized versus systemic immune therapy in melanoma patients (14, 15). Our studies confirm and extend this previous work by evaluating possible underlying mechanisms of IT administration of IC, as well as showing antitumor efficacy in an established measureable disease setting in a preclinical model. IHC infiltration data collected using the quantitative method that we developed are consistent with infiltration data collected by flow cytometry. Although the experimental design intended for each animal within a treatment group to be identical to one another, there is substantial heterogeneity within treatment groups, which is the topic of a separate article (R.K. Yang, N.A. Kalogriopoulos,

A.L. Rakhmilevich, E.A. Ranheim, S. Seo, K. Kim, K.L. Alderson, J. Gan, R.A. Reisfeld, S.D. Gillies, J.A. Hank, and P.M. Sondel, manuscript in preparation). The preclinical data presented in this report demonstrate several unique antitumor effects of IT-IC compared with equivalent doses of systemic IC. Flow cytometry analyses of IC delivery and retention show a substantial difference in the amount of IC present at initial time points at the tumor site between IT and i.v. administration. This direct exposure to greater concentrations of IT-IC at the tumor site between IT-IC and i.v.-IC treatment may be responsible, at least in part, for the different tumor-response rates and the different infiltration and expression patterns of TILs between the two treatment groups. These mechanisms of enhanced activity by localized IT treatment provide further justification for proceeding with clinical testing of IT-IC, potentially testing IT delivery of IC in patients with $GD2^+$ tumors, such as melanoma patients with metastatic disease having cutaneous, s.c., or readily injectable involved lymph nodes. Furthermore, the type of analyses presented in this preclinical report might also be conducted on biopsies of patient samples following IT-IC administration. Such immune monitoring by IHC and flow cytometry may become a potential means to assess the immunologic effects of immunocytokine treatment; if these parameters show correlation with antitumor effect, they may be considered indicators for prognosis of patients' response to IT-IC.

Acknowledgments

We thank Dr. Brett Yamane and Mark Baldeshwiler for help with experiments and Dr. Bartosz Grzywacz for helpful discussions.

Disclosures

The authors have no financial conflicts of interest.

References

1. Gillies, S. D., E. B. Reilly, K. M. Lo, and R. A. Reisfeld. 1992. Antibody-targeted interleukin 2 stimulates T-cell killing of autologous tumor cells. *Proc. Natl. Acad. Sci. USA* 89: 1428–1432 (PMID:1741398).
2. Lode, H. N., R. Xiang, N. M. Varki, C. S. Dolman, S. D. Gillies, and R. A. Reisfeld. 1997. Targeted interleukin-2 therapy for spontaneous neuroblastoma metastases to bone marrow. *J. Natl. Cancer Inst.* 89: 1586–1594 (PMID: 9362156).
3. Lode, H. N., R. Xiang, T. Dreier, N. M. Varki, S. D. Gillies, and R. A. Reisfeld. 1998. Natural killer cell-mediated eradication of neuroblastoma metastases to bone marrow by targeted interleukin-2 therapy. *Blood* 91: 1706–1715 (PMID: 9473237).
4. Xiang, R., H. N. Lode, C. S. Dolman, T. Dreier, N. M. Varki, X. Qian, K. M. Lo, Y. Lan, M. Super, S. D. Gillies, and R. A. Reisfeld. 1997. Elimination of established murine colon carcinoma metastases by antibody-interleukin 2 fusion protein therapy. *Cancer Res.* 57: 4948–4955 (PMID: 9354462).
5. Liu, Y., W. Zhang, L. H. Cheung, T. Niu, Q. Wu, C. Li, C. S. Van Pelt, and M. G. Rosenblum. 2006. The antimelanoma immunocytokine scFvMEL/TNF shows reduced toxicity and potent antitumor activity against human tumor xenografts. *Neoplasia* 8: 384–393 (PMID:16790087).
6. Yu, A. L., A. L. Gilman, M. F. Ozkaynak, W. B. London, S. G. Kreissman, H. X. Chen, M. Smith, B. Anderson, J. G. Villablanca, K. K. Matthay, et al; Children's Oncology Group. 2010. Anti-GD2 antibody with GM-CSF, interleukin-2, and isotretinoin for neuroblastoma. *N. Engl. J. Med.* 363: 1324–1334 (PMID: 20879881).
7. Osenga, K. L., J. A. Hank, M. R. Albertini, J. Gan, A. G. Sternberg, J. Eickhoff, R. C. Seeger, K. K. Matthay, C. P. Reynolds, C. Twist, et al; Children's Oncology Group. 2006. A phase I clinical trial of the hu14.18-IL2 (EMD 273063) as a treatment for children with refractory or recurrent neuroblastoma and melanoma: a study of the Children's Oncology Group. *Clin. Cancer Res.* 12: 1750–1759 (PMID: 16551859).
8. Shusterman, S., W. B. London, S. D. Gillies, J. A. Hank, S. D. Voss, R. C. Seeger, C. P. Reynolds, J. Kimball, M. R. Albertini, B. Wagner, et al. 2010. Antitumor activity of hu14.18-IL2 in patients with relapsed/refractory neuroblastoma: a Children's Oncology Group (COG) phase II study. *J. Clin. Oncol.* 28: 4969–4975 (PMID: 20921469).
9. King, D. M., M. R. Albertini, H. Schalch, J. A. Hank, J. Gan, J. Surfus, D. Mahvi, J. H. Schiller, T. Warner, K. Kim, et al. 2004. Phase I clinical trial of the immunocytokine EMD 273063 in melanoma patients. *J. Clin. Oncol.* 22: 4463–4473 (PubMed: 15483010).
10. Ribas, A., J. M. Kirkwood, M. B. Atkins, T. L. Whiteside, W. Gooding, A. Kovar, S. D. Gillies, O. Kashala, and M. A. Morse. 2009. Phase I/II open-label study of the biologic effects of the interleukin-2 immunocytokine EMD 273063 (hu14.18-IL2) in patients with metastatic malignant melanoma. *J. Transl. Med.* 7: 68–78 (PMID: 19640287).
11. Christ, O., S. Seiter, S. Matzku, C. Burger, and M. Zöller. 2001. Efficacy of local versus systemic application of antibody-cytokine fusion proteins in tumor therapy. *Clin. Cancer Res.* 7: 985–998 (PMID: 11309350).
12. Gillies, S. D., Y. Lan, B. Brunkhorst, W. K. Wong, Y. Li, and K. M. Lo. 2002. Bifunctional cytokine fusion proteins for gene therapy and antibody-targeted treatment of cancer. *Cancer Immunol. Immunother.* 51: 449–460 (PMID: 12202906).
13. Johnson, E. E., H. D. Lum, A. L. Rakhmilevich, B. E. Schmidt, M. Furlong, I. N. Buhtoiarov, J. A. Hank, A. Raubitschek, D. Colcher, R. A. Reisfeld, et al. 2008. Intratumoral immunocytokine treatment results in enhanced antitumor effects. *Cancer Immunol. Immunother.* 57: 1891–1902 (PMID: 18438664).
14. Weide, B., E. Derhovanessian, A. Pflugfelder, T. K. Eigentler, P. Radny, H. Zelba, C. Pföhler, G. Pawelec, and C. Garbe. 2010. High response rate after intratumoral treatment with interleukin-2: results from a phase 2 study in 51 patients with metastasized melanoma. *Cancer* 116: 4139–4146 (PMID:20564107).
15. Weide, B., T. K. Eigentler, A. Pflugfelder, U. Leiter, F. Meier, J. Bauer, D. Schmidt, P. Radny, C. Pföhler, and C. Garbe. 2011. Survival after intratumoral interleukin-2 treatment of 72 melanoma patients and response upon the first chemotherapy during follow-up. *Cancer Immunol. Immunother.* 60: 487–493 (PMID:21174093).
16. Vance, R. E., A. M. Jamieson, D. Cado, and D. H. Raulet. 2002. Implications of CD94 deficiency and monoallelic NKG2A expression for natural killer cell development and repertoire formation. *Proc. Natl. Acad. Sci. USA* 99: 868–873 (PMID: 11782535).
17. McMahon, C. W., A. J. Zajac, A. M. Jamieson, L. Corral, G. E. Hammer, R. Ahmed, and D. H. Raulet. 2002. Viral and bacterial infections induce expression of multiple NK cell receptors in responding CD8(+) T cells. *J. Immunol.* 169: 1444–1452 (PMID: 12133970).
18. Neal, Z. C., J. C. Yang, A. L. Rakhmilevich, I. N. Buhtoiarov, H. E. Lum, M. Imboden, J. A. Hank, H. N. Lode, R. A. Reisfeld, S. D. Gillies, and P. M. Sondel. 2004. Enhanced activity of hu14.18-IL2 immunocytokine against murine NXS2 neuroblastoma when combined with interleukin 2 therapy. *Clin. Cancer Res.* 10: 4839–4847 (PMID: 15269160).
19. Vance, R. E., J. R. Kraft, J. D. Altman, P. E. Jensen, and D. H. Raulet. 1998. Mouse CD94/NKG2A is a natural killer cell receptor for the nonclassical major histocompatibility complex (MHC) class I molecule Qa-1(b). *J. Exp. Med.* 188: 1841–1848 (PMID: 9815261).
20. Sondel, P. M., and J. A. Hank. 1997. Combination therapy with interleukin-2 and antitumor monoclonal antibodies. *Cancer J. Sci. Am.* 3(Suppl. 1): S121–S127 (PMID: 9457407).
21. Mulé, J. J., J. C. Yang, R. L. Afreniere, S. Y. Shu, and S. A. Rosenberg. 1987. Identification of cellular mechanisms operational in vivo during the regression of established pulmonary metastases by the systemic administration of high-dose recombinant interleukin 2. *J. Immunol.* 139: 285–294 (PMID: 3108401).
22. Voss, S. D., R. J. Robb, G. Weil-Hillman, J. A. Hank, K. Sugamura, M. Tsudo, and P. M. Sondel. 1990. Increased expression of the interleukin 2 (IL-2) receptor beta chain (p70) on CD56+ natural killer cells after *in vivo* IL-2 therapy: p70 expression does not alone predict the level of intermediate affinity IL-2 binding. *J. Exp. Med.* 172: 1101–1114 (PMID: 1698909).
23. Weil-Hillman, G., P. Fisch, A. F. Prieve, J. A. Sosman, J. A. Hank, and P. M. Sondel. 1989. Lymphokine-activated killer activity induced by *in vivo* interleukin 2 therapy: predominant role for lymphocytes with increased expression of CD2 and leu19 antigens but negative expression of CD16 antigens. *Cancer Res.* 49: 3680–3688 (PMID: 2471587).
24. Gubbels, J. A., B. Gadbaw, I. N. Buhtoiarov, S. Horibata, A. K. Kapur, D. Patel, J. A. Hank, S. D. Gillies, P. M. Sondel, M. S. Patankar, and J. Connor. 2011. Ab-IL2 fusion proteins mediate NK cell immune synapse formation by polarizing CD25 to the target cell-effector cell interface. *Cancer Immunol. Immunother.* 60: 1789–1800 (PMID: 21792658).
25. Buhtoiarov, I. N., Z. C. Neal, J. Gan, T. N. Buhtoiarova, M. S. Patankar, J. A. Gubbels, J. A. Hank, B. Yamane, A. L. Rakhmilevich, R. A. Reisfeld, et al. 2011. Differential internalization of hu14.18-IL2 immunocytokine by NK and tumor cell: impact on conjugation, cytotoxicity, and targeting. *J. Leukoc. Biol.* 89: 625–638 (PMID: 21248148).
26. Verneris, M. R., M. Karami, J. Baker, A. Jayaswal, and R. S. Negrin. 2004. Role of NKG2D signaling in the cytotoxicity of activated and expanded CD8+ T cells. *Blood* 103: 3065–3072 (PMID: 15070686).